Cold wire constant voltage anemometry to measure temperature fluctuations and its application in a thermoacoustic system

Sarah Cleve, Emmanuel Jondeau, Philippe Blanc-Benon, and Geneviève Comte-Bellot
Laboratoire de Mécanique des Fluides et d'Acoustique, UMR CNRS 5509, École Centrale de Lyon, Université de Lyon, 36 Avenue Guy de Collongue, 69134 Ecully Cedex, France

(Received 20 December 2016; accepted 25 March 2017; published online 11 April 2017)

The knowledge of temperature fluctuations is essential for most thermoacoustic systems. In the present paper, cold wire constant-voltage anemometry (CVA) to measure temperature fluctuations is presented. Corrections for the thermal inertia and for the end losses of the wire are applied during the post-processing. The correction for the thermal inertia of the cold wire is achieved by applying a time dependent thermal lag as proposed originally for a constant-current anemometry (CCA) system. This thermal lag is measured in parallel by a hot wire. The thermal end losses of the wires to their supports are also considered and approximate corrections are proposed. The procedure for the cold wire CVA is validated in the acoustic field of an acoustic resonator with wires of different lengths. A comparison between a CVA and a CCA measurement also confirms the CVA measurement. Furthermore, the proposed measurement procedure is applied close to the stack of a thermoacoustic refrigerator. Supposing a two-dimensional flow, the simultaneous measurement of velocity and temperature fluctuations is possible. This allows a detailed examination of the acoustic field close to the stack, including the study of the correlation between temperature and velocity. *Published by AIP Publishing.* [http://dx.doi.org/10.1063/1.4979823]

I. INTRODUCTION

In the context of thermoacoustic systems, it is desired to measure temperature fluctuations of a relatively small amplitude of the order of 1 °C and of a relatively high frequency, up to 1 kHz. As thermocouples are not appropriate to measure fluctuations, other methods are needed.

Recently, Penelet *et al.*[1] presented the measurement of a temperature field in a thermoacoustic oscillator using digital holographic interferometry. As this method is an optical method, it necessitates optical access to the test area.

The use of thermal anemometers is an intrusive measurement, but it does not need optical access. Operating a fine thermal wire at low overheat enables use of this wire as a resistance thermometer and to measure temperature fluctuations. This method is called the cold wire technique.[2] Until now, usually a cold wire has been operated by constant-current anemometry (CCA). In the present paper, the use of a prototype of a constant-voltage anemometer (CVA) is presented. The cold wire CVA system has the advantage of being an autonomous measurement unit and of supplying the possibility to implement hardware corrections. Advantages of a hardware correction were, for instance, discussed by Sarma[3] in the context of a hot wire anemometer. More details about CVA and CCA systems are discussed, for instance, by Comte-Bellot.[4]

Even though a fine wire, operated at extremely low overheat, is adapted to measure temperature fluctuations, some errors occur that can be corrected during the post-processing.

Most importantly, the thermal inertia of the wire necessitates the correction for its thermal lag. In the case of boundary layers or jets, the use of a mean value of the thermal lag, fitting the mean velocity and the mean wire overheat, is sufficient. In oscillating flows, a more elaborate method is needed. Berson *et al.*[5] proposed to use a time dependent thermal lag $\mathcal{M}_w(t)$, which is measured in parallel by a hot wire. This correction, initially proposed for a CCA system, is adapted here for a CVA measurement.

Another error which influences especially cold wire measurements is due to the so-called end losses, due to the heat lost by conduction towards the supports of the wire. The behavior of cold wires has been examined by several authors, among the first, Bremhorst and Gilmore[6] and Paranthoen *et al.*[7] Paranthoen *et al.*[7] examined the behavior of a wire to externally induced temperature fluctuations. They obtained a frequency response $H(f)$, which indicates that the amplitude measured by the wire diminishes when the frequency increases. It is important to note that all studies on the frequency response only cover non-zero mean flows. Purely oscillating flows have been investigated for the *microflown technique* (overview by de Bree[8] and mathematical model by van Honschoten *et al.*[9]). However, this technique uses the temperature difference between two closely placed wires. It does not conclude on the absolute temperature of single wires.

The theoretical background of cold wire anemometry as well as its corrections is discussed in Sec. II. The anemometers operating the cold and hot wires are presented in Sec. III. The method is then validated in the acoustic field of an acoustic resonator in Sec. IV. The results presented are notably those of the thermal lag $\mathcal{M}_w(t)$ and the temperature $T_w(t)$ as functions of time.

Lastly, in Sec. V, an exemplary application of the introduced measurement technique is presented. The acoustic field close to the stack of a thermoacoustic refrigerator has been analyzed. The use of two wires, a cold and a hot wire, allows

the parallel measurement of temperature fluctuations and velocity fluctuations. In particular, this allows the possibility to calculate the correlation between temperature and particle velocity.

II. COLD WIRE CVA MEASUREMENT AND ITS CORRECTION

A. Correction of the thermal inertia of a wire

The basic relation of thermal anemometry using metallic wires links the wire resistance R_w to the wire temperature T_w,

$$R_w = R_0\,(1 + \chi\,(T_w - T_0))\,, \tag{1}$$

where χ is the temperature coefficient of resistivity and R_0 the resistance of the wire at the reference temperature T_0. For an ideal cold wire devoid of thermal inertia and placed in a flow of instantaneous temperature $T_a(t)$, relation (1) gives

$$R^*_{wC}(t) = R_0\,(1 + \chi\,(T_a(t) - T_0))$$

or

$$T_a(t) - T_0 = \frac{R^*_{wC}(t) - R_0}{R_0\chi}. \tag{2}$$

The upper index $*$ refers to an ideal wire and the lower index wC refers to a cold wire, i.e., almost unheated. A real cold wire whose resistance R_{wC} is measured by the anemometer circuit differs from R^*_{wC}. The link between R_{wC} and R^*_{wC} may be approached by a first order differential equation (Bailly and Comte-Bellot[10]),

$$R^*_{wC}(t) = R_{wC}(t) + \mathcal{M}_w(t)\frac{\mathrm{d}R_{wC}(t)}{\mathrm{d}t}, \tag{3}$$

where $\mathcal{M}_w$ is the thermal lag of the wire. Berson *et al.*[5] showed in Appendix B that

$$\mathcal{M}_w(t) = \frac{m_w c_w}{\chi R_0}\frac{1}{f[U_n(t)]}, \tag{4}$$

where m_w is the mass of the wire, c_w the specific heat of the wire material, and $f[U_n(t)]$ a function of the velocity component U_n normal to the wire. $\mathcal{M}_w$ is clearly made of two independent factors: $m_w c_w/\chi R_0$ which is intrinsic to the wire and $1/f[U_n(t)]$ which depends on the incident flow.

The function $f[U_n(t)]$ is well known from its appearance in the heat balance of a hot wire. In the case of an ideal wire without thermal lag, this heat balance is

$$R^*_{wH}(t)I_{wH}(t)^2 = f[U_n(t)](R^*_{wH}(t) - R_a(t)), \tag{5}$$

where the Joule heating of the wire by the current I_{wH} equilibrates the convective heat loss of the wire. R_a is the resistance the wire would have at ambient temperature T_a. A relation between the expression $f[U_n]$ and the velocity U_n can be obtained by using King's law, then $f[U_n] = A + BU_n^m$, where A and B are constants and $m \approx 0.5$ for high aspect ratios length/diameter of the wire (Bailly and Comte-Bellot[10]). Equation (5) can be transformed for a wire fed by a constant voltage anemometer,

$$R^*_{wH}(t)\frac{{V^*_{wH}}^2}{(R^*_{wH}(t) + r_L)^2} = f[U_n(t)](R^*_{wH}(t) - R_a(t)), \tag{6}$$

where V_{wH} is the voltage across the hot wire kept constant and r_L the resistance of the lead and cable connecting the wire to the anemometer. For a real wire, some heat is stored by the wire. Equation (6) becomes

$$m_w c_w\frac{\mathrm{d}T_{wH}(t)}{\mathrm{d}t} = R_{wH}(t)I_{wH}(t)^2 - f[U_n(t)](R_{wH}(t) - R_a(t)) \tag{7}$$

and

$$\frac{m_w c_w}{\chi R_0}\frac{\mathrm{d}R_{wH}(t)}{\mathrm{d}t} = R_{wH}(t)I_{wH}(t)^2 - f[U_n(t)](R_{wH}(t) - R_a(t)). \tag{8}$$

The elimination of $f[U_n]$ between (6) and (8) gives

$$\frac{1}{V^2_{wH}}\frac{m_w c_w}{\chi R_0}\frac{\mathrm{d}R_{wH}}{\mathrm{d}t} = \frac{R_{wH}}{(R_{wH} + r_L)^2} - \frac{R_{wH} - R_a}{R^*_{wH} - R_a}\frac{R^*_{wH}}{(R^*_{wH} + r_L)^2}. \tag{9}$$

From this equation, R^*_{wH} can be obtained from the measured R_{wH}. Then, $1/f[U_n]$ can be obtained from Equation (6),

$$\frac{1}{f[U_n(t)]} = \frac{(R^*_{wH}(t) + r_L)^2}{V^2_{wH}}\frac{R^*_{wH}(t) - R_a(t)}{R^*_{wH}(t)}. \tag{10}$$

Note that this equation allows $f[U_n(t)]$ to be measured (with a hot wire) without knowing the actual flow velocity.

The factor $m_w c_w/\chi R_0$ is determined separately in a low-turbulence flow such as the potential cone of a jet studying the exponential decay of the anemometer output when a square wave perturbation is applied to the wire voltage while U_n is kept constant. See Ref. 11 for more details. The time constant M_{CVA} is equal to the time at which the signal has decayed by 63% and it is given for CVA by

$$M_{CVA} = \frac{m_w c_w}{\chi R_0}\frac{1}{f[U_n]}\frac{1 + a_w}{1 + 2a_w}LM \tag{11}$$

from the work of Comte-Bellot *et al.*[12] Using Equation (10) this gives

$$\frac{m_w c_w}{\chi R_0} = M_{CVA}V^2_{wH}\frac{1}{(R_{wH} + r_L)^2}\frac{1 + 2a_w}{a_w}\frac{1}{LM}, \tag{12}$$

where a_w is the wire overheat, $a_w = (R_{wH} - R_a)/R_a$, and LM a correction factor due to the cable connecting the wire to the anemometer (often $LM \approx 1$, see the work of Comte-Bellot *et al.*[12]).

Preliminary tests confirmed that neither $m_w c_w/\chi R_0$ nor $1/f[U]$ depends on the overheat of the wire. Furthermore, the value for $m_w c_w/\chi R_0$ remained constant for different flow velocities.

B. Correction of end losses

Previous publications (notably those by Berson *et al.*[5]) considered the aspect ratio $l/d \to \infty$. However, the wires have a finite aspect ratio. The resulting conduction along the wire leads to heat loss to the wire supports.

Paranthoen *et al.*[7] conducted experiments to study the frequency response $H(f)$ of different wires. They observed that $H(f)$ stays at a constant value H_p over a certain frequency

range for a given wire and a given incident velocity. Tsuji *et al.*[13] confirmed these observations by solving the equations of heat conduction numerically. Their results are available in terms of dimensionless quantities. Applied to our wire and Nusselt numbers, the plateau value H_p is estimated to be exact up to 500 Hz.

The plateau value H_p can be estimated by

$$H_p = 1 - 2\frac{l_c}{l}, \tag{13}$$

where l is the wire length and l_c the *cold wire length* defined by Betchov as

$$l_c = 0.5d\sqrt{\frac{k_w}{k_f}\frac{1}{\mathrm{Nu}}} \tag{14}$$

and also recalled by Bruun.[14] In definition (14), k_w and k_f are the thermal conductivities of the wire and fluid, respectively, and Nu is the Nusselt number. The Nusselt number can be calculated by an empiric law, for instance, by the one found by Collis and Williams,[15]

$$\mathrm{Nu} = 0.24 + 0.56\mathrm{Re}^{0.45}. \tag{15}$$

For the signals discussed in Section IV, the mean velocity magnitude is $U_n = 2.3\ \mathrm{ms}^{-1}$. Consequently, the mean Reynolds number is Re = 0.44 and the mean Nusselt number is Nu = 0.63. This leads to $H_p = 0.90$.

In this context, we propose to use H_p as a correction factor on the temperature signal, which gives

$$T_{a,\text{cor. end loss}}(t) = \frac{T_a(t)}{H_p}. \tag{16}$$

Note that an alternative method to calculate the Nusselt number can be found by extending its definition,

$$\mathrm{Nu} = \frac{R_{wH}I_{wH}^2}{\pi l k_f (T_{wH}^* - T_a)} = \frac{\chi R_a}{\pi l k_f} f[U], \tag{17}$$

which gives for a wire operated by CVA,

$$\mathrm{Nu} = \frac{\chi R_a}{\pi l k_f}\frac{V_{wH}^2}{(R_{wH}^* + r_L)^2}\frac{R_{wH}^*}{R_{wH}^* - R_a}. \tag{18}$$

III. THE ANEMOMETERS

A cold wire CVA system is used to measure temperature fluctuations and a hot wire CVA system is used in parallel to correct the thermal lag of the temperature measurement. The two anemometers used are described in this section.

The hot wire anemometer is a Model 4-600 CVA fabricated by Tao Systems, Inc. A simplified circuit is presented in Fig. 1. The response equation of this circuit is

$$\frac{V_{sH}(t)}{V_{wH}} = 1 + \frac{R_2}{R_{wH}(t) + r_L} + T_{cH}R_2\frac{\mathrm{d}}{\mathrm{d}t}\left(\frac{1}{R_{wH}(t) + r_L}\right). \tag{19}$$

In Eq. (19), V_{wH} is the voltage across the wire which is kept constant and V_{sH} is the output voltage of the hot wire CVA anemometer. The resistance $R_2 = R_{2a} + R_{2b}$ and the capacitance C_H are properties of the measurement unit. R_{wH} is the resistance of the wire and r_L is the resistance of the wire support plus cables. T_{cH} is the hardware-based time compensation offered by the electronic circuit. It can partly compensate the thermal inertia of the wire and is expressed by

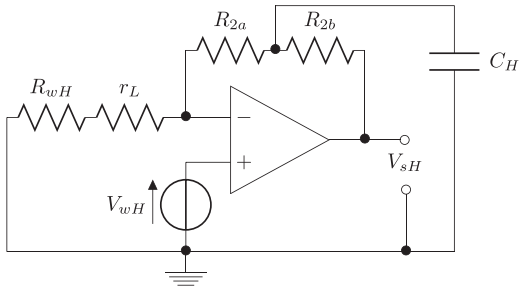

FIG. 1. Simplified hot wire CVA circuit.

$$T_{cH} = \frac{R_{2a}R_{2b}}{R_2}C_H. \tag{20}$$

The anemometer settings provide a choice of T_{cH}-values. Advantages of a system with a partial hardware correction compared to a system with a software correction alone are discussed by Sarma.[3]

The settings used for the hot wire circuit are $R_2 = 118\ \Omega$ and $T_{cH} = 100\ \mu$s. The applied voltage is $V_{wH} \approx 800$ mV; the current through the wire, therefore, is of the order of $I_{wH} \approx 35$ mA depending on the wire resistance.

The cold wire anemometer is a 5001 CVA prototype designed and fabricated by Tao Systems, Inc. The simplified circuit diagram is presented in Fig. 2. Neglecting a term $R_B C_C \mathrm{d}V_s/\mathrm{d}t$ which is small compared to V_s, the corresponding response equation is

$$\frac{V_{sC}(t)}{V_{wC}} = 1 + \frac{2R_f}{R_{wC}(t) + r_L} + 2R_f T_{cC}\frac{\mathrm{d}}{\mathrm{d}t}\left(\frac{1}{R_{wC}(t) + r_L}\right), \tag{21}$$

where V_{wC} is the voltage across the wire which is kept constant and V_{sC} is the output voltage of the cold wire CVA anemometer. R_{wC} is the resistance of the cold wire. The resistance $R_f = 20\ \mathrm{k}\Omega$ is a constant of the system. The voltage applied is $V_{wC} \approx 8$ mV. The current through the wire is of the order of $I_{wC} \approx 0.3$ mA depending on the wire resistance. The hardware-based time compensation T_{cC} is given by

$$T_{cC} = C_C\left(\frac{R_f}{2} + R_B\right), \tag{22}$$

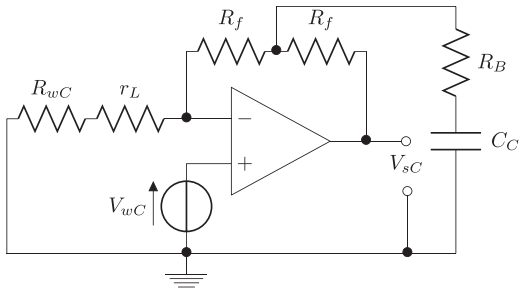

FIG. 2. Simplified cold wire CVA circuit.

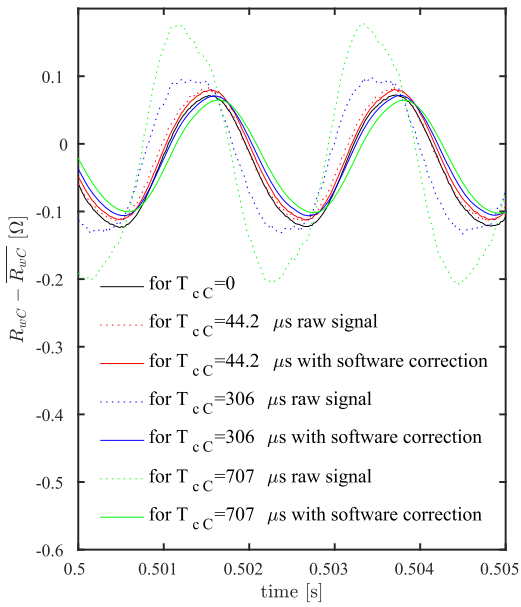

FIG. 3. Comparison of the cold wire resistance for different hardware corrections T_{cC} for the raw signal (pointed lines) and after applying the software correction (continuous lines) for a wire of aspect ratio $l/d \approx 1000$.

where the capacitance C_C and the resistance R_B can be adjusted to obtain T_{cC}-values ranging from 0 to 707 μs. Fig. 3 presents the measured wire resistance for different T_{cC}-values. The wire is placed in an acoustic field. When the internal hardware compensation is applied, the raw signal R_{wC} naturally exhibits a large amplitude and a phase advance (pointed lines in Fig. 3). This is particularly clear for $T_{cC} = 707$ μs. After the software correction (by solving differential equation (21)), a good agreement can be observed between the final results (continuous lines in Fig. 3). The small differences could be explained by the simplification and the incertitude of the components of the electrical circuit.

In Secs. IV and V, $T_{cC} = 0$ has been chosen to ease the data processing. In this case, response Equation (21) becomes

$$\frac{V_{sC}(t)}{V_{wC}} = 1 + \frac{2R_f}{R_{wC}(t) + r_L} \quad . \tag{23}$$

During the post-processing, the differential equations (3), (9), and (19) are solved using an explicit first order numerical procedure. This is adequate as the sampling frequency is sufficiently high.

IV. VALIDATION OF THE MEASUREMENT PROCEDURE

A. Setup for the validation in an empty resonator

The procedure introduced in Sec. II has been validated in an acoustic resonator. The setup is presented in Fig. 4. The resonator consists of a round rigid tube with a diameter of 30 mm. The length of the tube is 150 mm. A connecting element links the tube to the loudspeaker so that the total length of the resonator sums up to 190 mm. At $x = 0$, the resonator is closed by a rigid plate, through which the sensor of a thermal anemometer can be inserted. At $x = 7$ mm, a Brüel and Kjær 4938 1/4 in. reference microphone is placed flush with the wall. The resonator is designed to be a $\lambda/4$-resonator. A

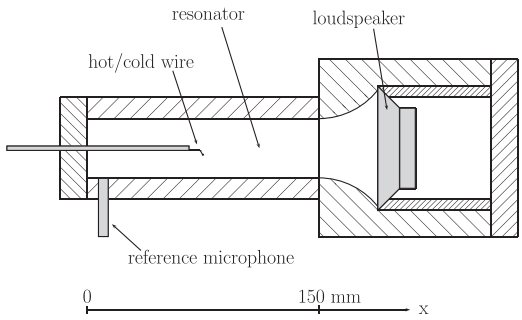

FIG. 4. A small resonator used for the validation procedure of the cold wire technique.

resonance frequency of $f_{res} \approx 460$ Hz has been obtained using a sine-sweep-excitation.

For the validation, three anemometry sensors of different lengths were fabricated in-house. The wire material is tungsten with 7% to 10% platinum. Their resistivity is of $5.5 \cdot 10^{-8}$ Ω m and their temperature coefficient of resistivity is of 0.0037 K^{-1}. The diameter of the wire is about 3 μm and the sensors have an aspect ratio $l/d \approx 500$, 1000, and 2000. Their reference resistances are $R_0 = 10.4$ Ω, 22.4 Ω, and 43.3 Ω at 22.1 °C. For all wires, the value $m_w c_w/\chi R_0 \approx 7 \cdot 10^{-7}$ A^2s was obtained in preliminary tests.

In the empty resonator, the theoretical evolutions of the temperature and of the particle velocity can be calculated from the microphone measurement. These theoretical values serve as references for the measured values. The reference pressure in the resonator is 3000 Pa. The anemometer output was sampled at 51.2 kHz.

For the results presented in this section, the same wire was first used as a hot and then as a cold wire. During the post-processing, corrections were applied at the corresponding phase of the oscillation.

B. Inertia correction

As the thermal lag $\mathcal{M}_w$ plays an important role in the inertia correction, it is presented in Fig. 5 for the sensor position $x = 70$ mm in the resonator.

In Fig. 6, the theoretical temperature evolution and the uncorrected and corrected temperature fluctuations for the three sensors are presented for the sensor position $x = 70$ mm.

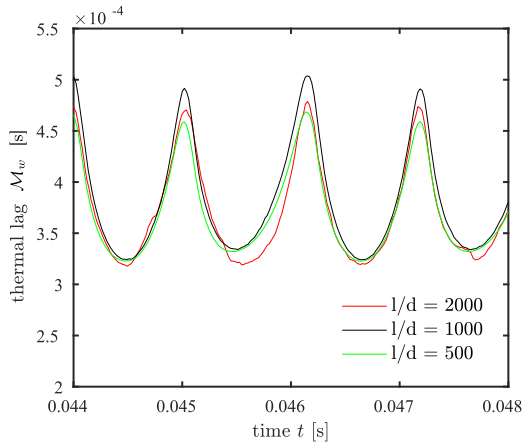

FIG. 5. Thermal lag $\mathcal{M}_w(t)$ as a function of time for $x = 70$ mm.

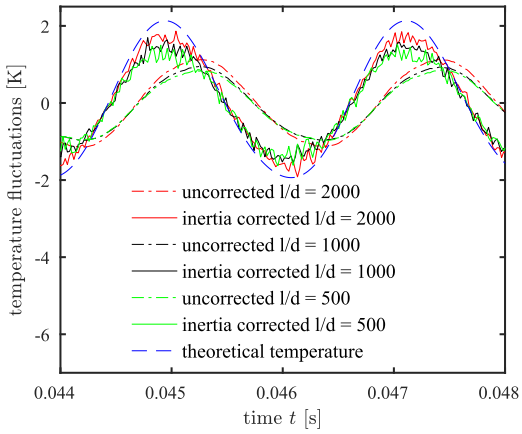

FIG. 6. Instantaneous temperature fluctuations—uncorrected, inertia corrected, and theoretical—as a function of time for $x = 70$ mm.

The theoretical phase of the temperature signal is well recovered from the corrected wire signals. Concerning the amplitude, a slight mismatch subsists between theory and corrected measurements. This mismatch is decreasing with increasing wire length.

The results at the sensor position $x = 70$ mm presented in Figures 5 and 6 are representative for all measurement positions. Fig. 7 shows the amplitude of the temperature fluctuations for all investigated points. It can be confirmed that the inertia correction is more efficient for longer wires.

C. End loss correction

The results of the end loss correction plus the inertia correction are presented in Fig. 8 compared to the results from the inertia correction alone (see Fig. 7). It can be observed that the amplitudes of these corrected signals measured with the three different wires become comparable within 5% discrepancy. Note, however, that a slight difference to theoretical values persists. One potential reason for this difference which is visible in Fig. 8 is that the plateau value H_p is originally established for flows with positive mean flow velocities. In our resonator, the flow is purely oscillatory. The occurrence of zero velocity corresponds to temperature extrema so that the value used for H_p can be questionable at those instants.

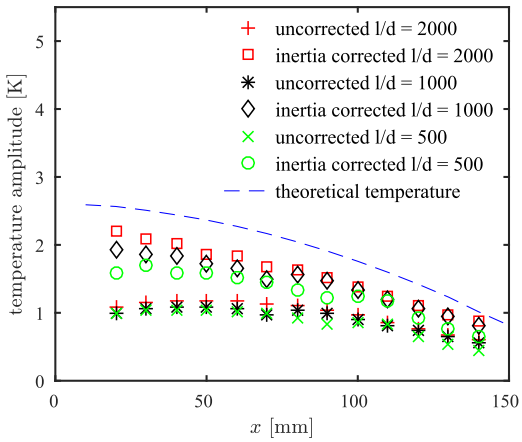

FIG. 7. Amplitudes of temperature fluctuations—uncorrected, inertia corrected, and theoretical—for the different positions in the resonator.

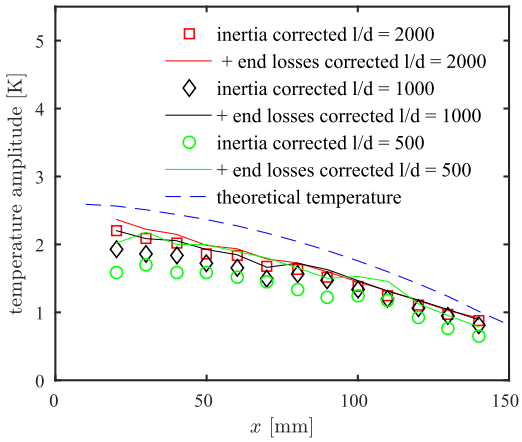

FIG. 8. Amplitudes of temperature fluctuations—inertia corrected, inertia and end losses corrected, and theoretical—for the different positions in the resonator.

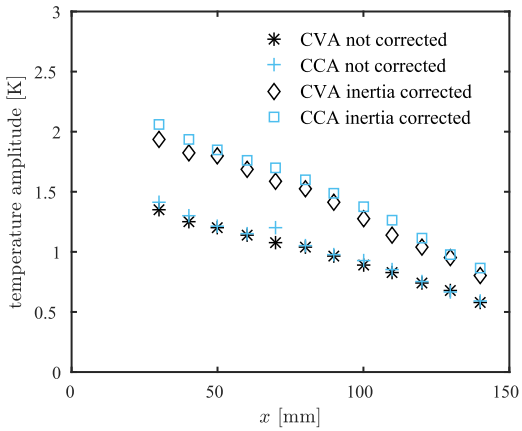

FIG. 9. Comparison between CVA and CCA measurements with a cold wire: amplitudes of temperature fluctuations for the different positions in the resonator.

Further reasons for this difference, albeit with a smaller impact, include the measurement uncertainty of $m_w c_w/\chi R_0$ and possible nonlinearities in the resonator due to a high drive ratio (compared to the work of Berson *et al.*[5]).

D. Comparison with CCA measurement

The cold wire CVA system is a prototype and no other temperature measurement by a cold wire CVA has been reported in the literature. As it is, hence, the first time that this has been conducted, a comparison with a CCA Dantec module 90C20 has been performed. Uncorrected results are compared to inertia corrected results in Fig. 9. A good agreement between the two measurements can be observed.

V. APPLICATION CLOSE TO THE STACK OF A THERMOACOUSTIC REFRIGERATOR

A. Experimental setup

The measurement of temperature fluctuations together with velocity fluctuations has been performed close to the stack of a thermoacoustic refrigerator. The experimental setup is presented in Fig. 10.

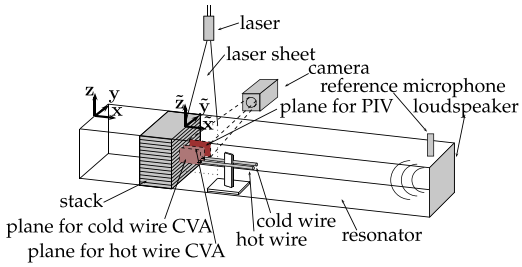

FIG. 10. Experimental setup with PIV and both cold and hot wire anemometry.

The refrigerator consists of a stack of glass plates inside a $\lambda/2$-resonator with a 80 mm wide square section and with a length of 860 mm. The resonance frequency in the presence of the stack is 195 Hz. A Brüel and Kjær 4938 1/4 in. reference microphone is placed at $x = 833$ mm. The middle of the stack is placed at $x = 140$ mm. This distance is retaken from Lotton *et al.*,[16] who used a similar setup. The reference pressure inside the resonator is 1500 Pa for the presented measurements.

The examined stack configuration presented here is with plates of $d = 1$ mm thickness and $e = 1$ mm spacing. A sketch is presented in Fig. 11.

Due to the thermoacoustic effect, the right end of the stack in the present setup will be cooled down and the left end of the stack will be heated up. Close to the cold end of the stack, hot and cold wire anemometry and time resolved particle image velocimetry (PIV) are performed. The PIV measurement has been used additionally to the hot wire anemometry as a means of validation for the velocity field. Note that cold wire measurement and PIV measurement could not be conducted at the same time due to an effect of the tracer particles on the cold wire. The hot wire measurement is not influenced by the tracer particles.

Three parallel lateral planes are used: one for the PIV measurement, one for the hot wire CVA measurement, and one for the cold wire CVA measurement. The separation of the planes is necessary in order to eliminate any interaction between the different measurement techniques. The PIV laser has such an intensity that it would simply heat the hot wire if the wire was placed too close to the laser sheet. As for the interaction between the hot wire and the cold wire, preliminary studies showed that with $V_{wH} = 800$ mV up to about 3 mm distance between the two wires, an effect of the hot on the cold wire can be observed. Hence, a setup with three parallel lateral planes is used. The spacing between the planes is about 15 mm. The parallel planes suppose a two-dimensional acoustic field in

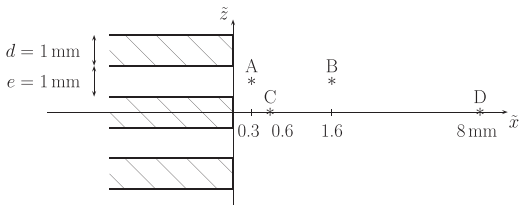

FIG. 11. Stack configuration and presented points in Sec. V B: Point A is situated at $\tilde{z} = (e + d)/2 = 1$ mm and $\tilde{x} = 0.3$ mm from the stack, point B at $\tilde{z} = (e + d)/2 = 1$ mm and $\tilde{x} = 1.6$ mm, point C at $\tilde{z} = 0$ and $\tilde{x} = 0.6$ mm, and point D at $\tilde{z} = 0$ and $\tilde{x} = 8$ mm.

which all three planes are considered to be equivalent. This assumption has been shown to be sufficiently correct, for instance, by Berson.[17]

During the measurement, the two CVA sensors are moved simultaneously with a linear piezoelectric device which allows steps of less than 0.1 mm. With the two sensors well adjusted before the measurement, they will always be at the same point (x, z) only separated by about 15 mm in the y-direction.

The two wires used for the measurement are similar to the wire of aspect ratio $l/d \approx 1000$ as described in Sec. IV A. In the following, the reference resistances (at 21.8 °C) of the cold and the hot wire are 23.6 Ω and 23.4 Ω, respectively. Preliminary tests showed that the wire properties are similar enough to apply the thermal lag measured by the hot wire directly on the cold wire without any factor of adjustment.

The sampling frequency of the CVA measurement is 51.2 kHz. The sampling frequency of the PIV measurement is 3.2 kHz. The signal length is 1 s.

B. Results in the empty resonator and close to the stack

Reference measurements in the empty resonator as well as measurements with the stack will be presented in the following. All measurements are phase-averaged over 180 periods.

1. Velocity

In preliminary tests on the empty resonator, the velocity signal given by PIV, the velocity signal calculated from the microphone, and the velocity deduced from the hot-wire CVA have been compared. In order to calibrate the hot-wire CVA, we use the PIV data. In Fig. 12 the results for the rectified velocity $|U_x|$ are presented. Note that for an empty resonator the velocity is only along the x-axis. Possible reasons for the slight asymmetry of the velocity signal in a resonator, which can also be observed in Fig. 12, are, for example, discussed by Jerbi *et al.*[18] Those authors suggest the presence of a mean flow, hence acoustic streaming, that could be responsible for the asymmetry of the CVA signal.

The following measurements have been performed close to the cold end of the stack, which is situated at $x = 180$ mm.

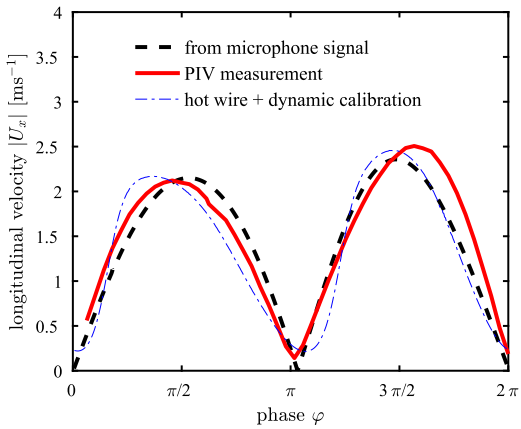

FIG. 12. Phase-average of the rectified U_x velocity in the empty resonator measured with PIV, calculated from the microphone signal and obtained from hot wire signal after calibration with the PIV signal for $x = 180$ mm.

A local coordinate system has been introduced in Fig. 10 with $\tilde{x} = 0$ at the end of the stack.

In Fig. 13, the phase-averaged signals for some measurement points close to the stack are presented to compare PIV measurement and hot wire CVA measurement for the velocity magnitude $U_n = \sqrt{U_x^2 + U_z^2}$, which is normal to the wire and already introduced in Section II. For a better understanding, the U_x-component obtained by PIV measurement is presented in the third plot. In all figures, a reference signal is presented. This reference corresponds to the theoretical particle velocity, which can be calculated from the microphone signal in an empty resonator.

The signals at points A and B are measured at the position $\tilde{z} = (e+d)/2 = 1$ mm. The interval 0 to π corresponds to the jet when the air flows out of the stack ($U_x > 0$). The interval π to 2π corresponds to air flowing back into the stack ($U_x < 0$). Point C represents the position $\tilde{z} = 0$, where recirculation is visible behind the plates of the stack. Therefore, its velocity profile is more complex. Far from the stack at point D, the velocity profile approaches the approximately symmetric profile of an empty resonator. The slight delay compared to the theoretical signal has already been observed before by Poignand *et al.*[19]

Most importantly, the good agreement between the CVA signals and the PIV signals allows the hypothesis that the hot wire CVA correctly measures the velocity field. This is important regarding the correction of temperature measurement

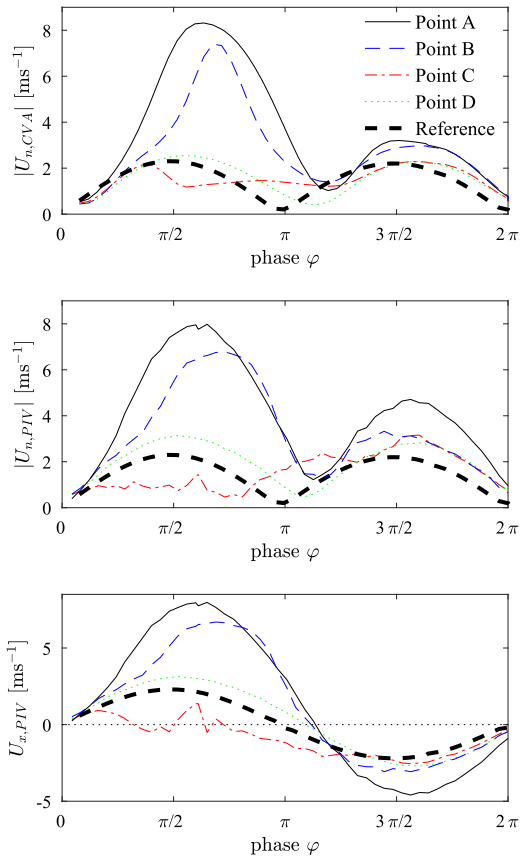

FIG. 13. Phase-averaged velocity magnitude $|U_n|$ obtained by CVA (upper plot) and PIV (central plot) as well as velocity U_x obtained by PIV (lower plot) for chosen points close to the stack. For their location refer to Figure 11.

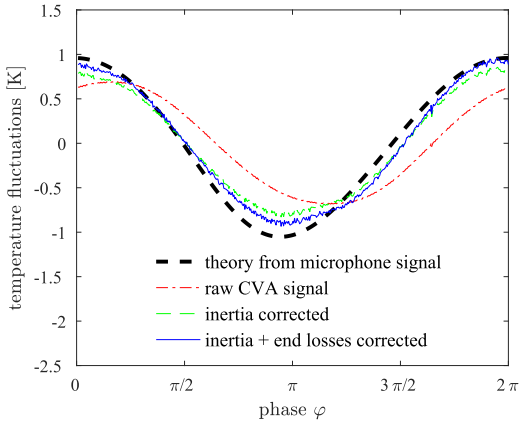

FIG. 14. Phase-averaged temperature fluctuations in the empty resonator calculated from the microphone signal and measured with cold wire CVA—uncorrected, inertia corrected, inertia and end losses corrected at the position $x = 180$ mm.

using the thermal lag calculated from the hot wire CVA measurements. Discrepancies at individual points can be explained by the following aspects: a small error may be due to the positioning of the CVA sensor with the movable device. Moreover, the stack had to be repositioned between the PIV measurement and the CVA measurement.

2. Temperature

In Fig. 14, the temperature measurement at $x = 180$ mm is presented for the empty resonator. As for the small resonator, a sinusoidal signal is obtained. In the inertia and end loss corrected signal, both amplitude and phase agree well with the theoretical temperature signal.

Close to the stack of the thermoacoustic refrigerator, the same measurement points as before are presented in Fig. 15. The value $\theta(t) = T(t) - \overline{T}_a$ is the temperature difference between the measured temperature and the mean temperature without the stack, hence the ambient temperature.

Once again, the result for point D far from the stack is very similar to the temperature signal received in the empty resonator. The largest alteration of the temperature signal can be observed for points A and B in the extension of the spacing between the plates of the stack.

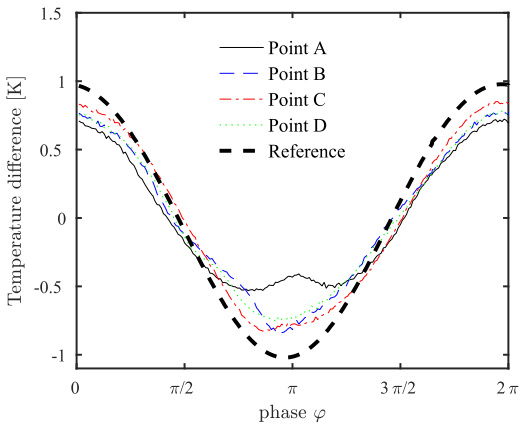

FIG. 15. Phase-averaged temperature fluctuations for chosen points close to the stack. For their location refer to Figure 11.

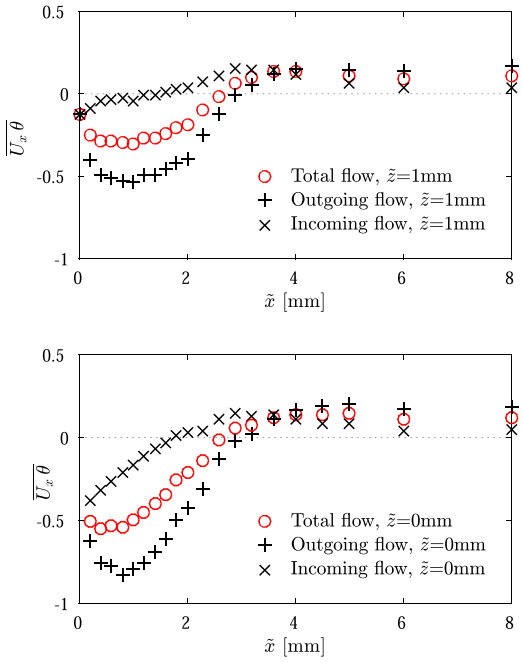

FIG. 16. Product $\overline{U_x(t)\theta(t)}$ for different positions $\tilde{x}$ for the position $\tilde{z} = (d + e)/2 = 1$ mm in the upper plot and for $\tilde{z} = 0$ in the lower plot.

A model for temperature fluctuations developed by Gusev *et al.*[20] predicts a nonlinear character of the temperature oscillations close to the stack. Berson *et al.*[21] and Penelet *et al.*[1] experimentally confirmed the appearance of harmonics. Even though no harmonic decomposition has been made in the present study, Figure 15 strongly supports the hypothesis of nonlinearities in the temperature signal clearly visible for point A.

3. Correlation between temperature and velocity

Detailed equations to describe energy transfer in a thermoacoustic system are established by Marx and Blanc-Benon.[22] The main quantity of interest is the enthalpy flux in the longitudinal direction

$$h_x = \overline{\rho_0 c_p U_x(t)\theta(t)}. \tag{24}$$

We therefore present the result of the product $\overline{U_x(t)\theta(t)}$ in Fig. 16 for different measurement points close to the stack.

As the hot wire measures the velocity normal to the wire and cannot separate the velocity components, we use for the U_x-signal the velocity obtained by the PIV measurement. This allows also a separation into an incoming and an out-flowing part. Far from the stack, the difference between the product $\overline{U_x(t)\theta(t)}$ for the incoming and the out-flowing part is zero. No energy is transported. Close to the stack, however, the total signal is not equal to zero. Therefore, according to the stack configuration sketched in Figures 10 and 11, enthalpy travels in the negative $\tilde{x}$-direction from the ambient air in the resonator to the cold entrance of the stack. The influence of the stack can be observed up to about 3.5 mm. This corresponds well to the distance of twice the acoustic displacement $2d_{ac} = 2U_x/2\pi f$ found by Berson *et al.*[23]

VI. CONCLUSION

Temperature fluctuations were measured using a CVA prototype specially conceived and built for cold wires. During the post-processing, the thermal inertia, by a simultaneous hot wire measurement, and the end losses were corrected. Taking into account different parameters such as the length of the wire, the method was validated in an acoustic resonator.

The technique was applied close to the stack of a thermoacoustic system. With a cold and a hot wire, the temperature and velocity fluctuations are obtained simultaneously. For the product $\overline{U_x(t)\theta(t)}$, we used the velocity-component U_x given by the PIV-measurement. These first results show that it is possible to measure the enthalpy flux which is a characteristic of thermal energy transfer in thermoacoustic devices.

ACKNOWLEDGMENTS

The authors thank Dr. Siva Mangalam, Arun Mangalam, and the engineers of Tao of Systems Integration, Inc. who have provided the cold wire CVA prototype.

This work has been conducted with the Labex *CeLyA* of the *Université de Lyon* supported by *l'Agence Nationale de la Recherche* (Nos. ANR-10-LABX-0060/ANR-11-IDEX-0007).

[1] G. Penelet, M. Leclercq, T. Wassereau, and P. Picart, Exp. Therm. Fluid Sci. **70**, 176 (2016).
[2] S. Corrsin, Rev. Sci. Instrum. **18**, 469 (1947).
[3] G. R. Sarma, Rev. Sci. Instrum. **69**, 2385 (1998).
[4] G. Comte-Bellot, in *Handbook of Experimental Fluid Mechanics*, edited by C. Tropea, A. L. Yarin, and J. F. Foss (Springer, 2007), pp. 229–287.
[5] A. Berson, G. Poignand, P. Blanc-Benon, and G. Comte-Bellot, Rev. Sci. Instrum. **81**, 015102 (2010).
[6] K. Bremhorst and D. Gilmore, Int. J. Heat Mass Transfer **21**, 145 (1978).
[7] P. Paranthoen, C. Petit, and J. Lecordier, J. Fluid Mech. **124**, 457 (1982).
[8] H.-E. de Bree, Acta Acust. Acust. **89**, 163 (2003).
[9] J. van Honschoten, G. Krijnen, V. Svetovoy, H.-E. de Bree, and M. Elwenspoek, in *The 14th IEEE International Conference on Micro Electro Mechanical Systems, 2001, MEMS 2001* (IEEE, 2001), pp. 523–526.
[10] C. Bailly and G. Comte-Bellot, *Turbulence* (Springer, 2015).
[11] A. Mohammed-Taifour, J. Weiss, A. Sadeghi, J. Vétel, E. Jondeau, and G. Comte-Bellot, Exp. Fluids **56**, 174 (2015).
[12] G. Comte-Bellot, J. Weiss, and J.-C. Béra, Rev. Sci. Instrum. **75**, 2075 (2004).
[13] T. Tsuji, Y. Nagano, and M. Tagawa, Exp. Fluids **13**, 171 (1992).
[14] H. H. Bruun, *Hot-Wire Anemometry-Principles and Signal Analysis* (Oxford Science Publications, 1995).
[15] D. Collis and M. Williams, J. Fluid Mech. **6**, 357 (1959).
[16] P. Lotton, P. Blanc-Benon, M. Bruneau, V. Gusev, S. Duffourd, M. Mironov, and G. Poignand, Int. J. Heat Mass Transfer **52**, 4986 (2009).
[17] A. Berson, "Vers la miniaturisation des réfrigérateurs thermoacoustiques: Charactérisation du transport non-linéaire de chaleur et des écoulements secondaires," Ph.D. thesis, No. 2007-41, École Centrale de Lyon, 2007.
[18] F. J. Jerbi, G. Huelsz, and S. Kouidri, Flow Meas. Instrum. **32**, 41 (2013).
[19] G. Poignand, E. Jondeau, and P. Blanc-Benon, in *17th AIAA/CEAS Aeroacoustics Conference (32nd AIAA Aeroacoustics Conference)* (AIAA, 2011), p. 2932.
[20] V. Gusev, P. Lotton, H. Bailliet, S. Job, and M. Bruneau, J. Acoust. Soc. Am. **109**, 84 (2001).
[21] A. Berson, G. Poignand, P. Blanc-Benon, and G. Comte-Bellot, Int. J. Heat Mass Transfer **54**, 4730 (2011).
[22] D. Marx and P. Blanc-Benon, AIAA J. **42**, 1338 (2004).
[23] A. Berson, M. Michard, and P. Blanc-Benon, Heat Mass Transfer **44**, 1015 (2008).